Journal of Mammalian Evolution, Vol. 12, Nos. 1/2, June 2005 (© 2005)
DOI: 10.1007/s10914-005-4861-0

Anatomy of the Cranial Endocast of the Bottlenose Dolphin, *Tursiops truncatus*, Based on HRXCT

Matthew W. Colbert,[1,4] Rachel Racicot,[1,3] and Timothy Rowe[1,2]

Endocranial surfaces, volumes, and interconnectivities of extant and fossil odontocetes potentially offer information on the general architecture of the brain and on the structure of the specialized cetacean circulatory system. Although conventional methods for acquiring such data have generally involved invasive preparation of the specimen, particularly in the case of fossils, new tomographic technologies afford nondestructive access to these internal morphologies. In this study we used high-resolution X-ray computed tomography (HRXCT) to scan a skull of the extant *Tursiops truncatus* (Cetacea: Odontoceti). We processed the data to reveal the cranial endocast and details of internal skeletal architecture (data at www.digimorph.org). Major features that can be discerned include aspects of the specimen's hypertrophied retia mirabilia, the major canals and openings of the cranial cavity, and the relationship of the brain and endocranial circulatory structures to the surrounding skeleton. CT data also provide information on the shape of the brain that may be lost in conventional anatomical preparations, and readily provide volumetric and linear measurements of the endocast and its individual segments. These results demonstrate the utility of HRXCT for interpreting the internal cranial anatomy of both extant and fossil cetaceans.

KEY WORDS: *Tursiops*, endocast, computed tomography.

INTRODUCTION

Odontocete skulls are drastically modified relative to the general mammalian condition. External evolutionary novelties include a "telescoped" morphology (Miller, 1923), which involves the posterior repositioning of anterior cranial bones and postero-dorsal positioning of the nares to form the "blowhole," and bilateral asymmetry. The relationship of these cranial modifications to evolution of an aquatic life history has been widely discussed (e.g., Moore, 1981; Novacek, 1993; Fordyce and de Muizon, 2001).

Internal cetacean skull architecture is also asymmetrical and shows the effects of telescoping. Additionally, internal osteology reflects their large brain size and provides evidence of evolutionary transformations in relative importance of the different peripheral sensory inputs (Breathnach, 1960; Morgane and Jacobs, 1972; Morgane *et al*., 1980; Ridgway, 1990).

[1] Jackson School of Geosciences, The University of Texas at Austin, Austin, Texas, USA.
[2] Texas Memorial Museum, The University of Texas at Austin, Austin, Texas, USA.
[3] Present address: Biology Department, San Diego State University, San Diego, California 92182, USA.
[4] To whom correspondence should be addressed at Geological Science Department, 1 University Station C1100, Austin, Texas 78712-0254, USA. E-mail: colbert@mail.utexas.edu

For example, whales lose the olfactory bulb and tract, and the rhinencephalon comprises a relatively much smaller portion of the brain, reflecting diminution of olfactory signal importance in whale life history strategies compared to most terrestrial mammals. The internal surfaces and passageways of the skull also preserve traces of a suite of features related to the derived and elaborated circulatory system of whales. The most prominent are hypertrophied local networks of blood vessels known as retia mirabilia, which are involved in diving physiology (Viamonte *et al*., 1968; Morgane and Jacobs, 1972; Vogl and Fisher, 1981a,b; Melnikov, 1997; Geisler and Lou, 1998).

Insofar as precise internal geometries of the endocranial spaces reflect the structure of the brain, its peripheral sensory systems, and its vascular system, students of whale evolution have long been interested in this region of the skeleton, and in naturally occurring and artificially created casts of the endocranial cavity (Edinger, 1955; Jerison, 1973; Barnes, 1985; Glezer *et al*., 1988; Geisler and Lou, 1998; Gingerich, 1998; Marino *et al*., 2003b). In spite of a relatively rich fossil record, however, natural whale endocasts are rare and the internal anatomy of the skull is poorly known in most species. In the past, access to the endocranial region of both fossil and Recent specimens has generally required destructive techniques to which curators rarely accede.

The problems of observing and measuring this region are diminishing as several digital technologies, particularly magnetic resonance imaging (MRI), medical X-ray computed axial tomography (CAT), and the derivative technology known as high-resolution X-ray computed tomography (HRXCT), have been increasingly applied to Recent and fossilized specimens of whales and other mammals (Conroy and Vannier, 1984; Rowe *et al*., 1995, 2005; Rowe 1996a,b; Joeckel, 1998; Marino *et al*., 2003a,b). HRXCT, the basis for the present report, uses higher energy X-rays, finer detectors, and longer imaging times than medical CT scanners to nondestructively image the interior of opaque objects. Accordingly, HRXCT can image denser objects, and can achieve orders of magnitude better resolution than CAT scanning (Carlson *et al*., 2003). As in other tomographic techniques, results of the scan comprise a series of contiguous digital "slices," that can be resectioned along any axis, rendered as three-dimensional volumes, and animated (Table I). These data can also be processed to visualize "segments" of the original volume, such as the cranial endocast (Fig. 1), and to provide both linear and volumetric measurements (Table II).

In this report, we evaluate the correspondence between literature descriptions of the odontocete brain and circulatory system to a digital cranial endocast that we isolated from

Table I. Supplementary Online Resources[a]

3D rendered animations available in "additional imagery" section of webpage
• Rotations of semitransparent skull, showing contained endocast
• Rotations of semitransparent skull, showing contained circulatory segment
• Rotations of entire endocast, including all segments, around the coronal, horizontal, and sagittal axes
• Rotations of circulatory segment around the coronal, horizontal, and sagittal axes
• Rotation highlighting bone density contrast in the skull
Standard imagery section of webpage
• 3D rotations of the skull around the coronal, horizontal, and sagittal axes
• Slice movies of the skull along the coronal, horizontal, and sagittal axes
• Dynamic cutaway movies of the skull along the coronal, horizontal, and sagittal axes

[a] All imagery available at *Tursiops truncatus* webpage on the "Digital Morphology" website, www.digimorph.org/specimens/tursiops_truncatus.

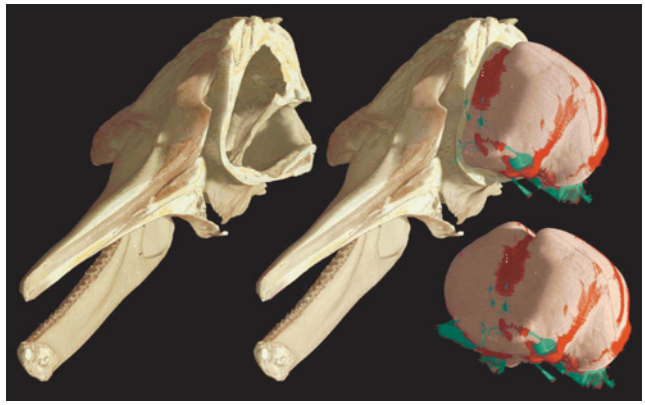

Fig. 1. 3D renderings of the skull and endocast illustrating the "segmented" cranial endocast. The digitally sectioned skull on the left illustrates the skull and cranial cavity without the endocast, while the top right image shows the sectioned skull with the digital endocast in place. The lower right image shows the endocast isolated from the skull. The total skull length, including the dentaries is 56.5 mm along the scan axis.

HRXCT scan data of a skull of *Tursiops*, the bottlenose dolphin. Attention is focused on features that can be identified on the HRXCT endocast, and on the relationship of these features to the surrounding skeleton, because these are potential sources of data for paleontologists. *Tursiops* was chosen as the subject of our study as it is perhaps the best-studied cetacean (Leatherwood and Reeves, 1990), and its central nervous system is well described, largely because of widespread interest in whale intelligence (e.g., see Marino *et al*., 2001, and references therein). Previous descriptions of the brain and circulatory system of *Tursiops* have been based on standard dissection techniques (Breathnach, 1960; Fraser and Purves, 1960; Galliano *et al*., 1966; Viamonte *et al*., 1968; Morgane and Jacobs, 1972; Morgane *et al*., 1980; Ridgway, 1990); injection of the circulatory system (Fraser and Purves, 1960; Viamonte *et al*., 1968; Morgane and Jacobs, 1972); and MRI analysis of isolated brains (Marino *et al*., 2001). Much other work is available on the central nervous system and cranial circulatory system of other cetaceans, and medical CAT scanners have been used to investigate the endocasts of a collection of fossil and Recent cetaceans (Marino

Table II. Volumetric and Linear Measurements

Segment	Volume (cm^3)
Neural	
Full volume	2048.23
Eroded 0.4 mm	1999.84
Eroded 0.8 mm	1954.27
Circulatory	64.36
Penetrations	19.29
Neural segment[a]	
Maximum width (cm)	19.0
Maximum height (cm)	16.4
Maximum length (cm)	16.0

[a] All measurements taken orthogonal to scan axis.

et al., 2003b), including a fossil archaeocete (Marino *et al*., 2000). This literature provides a framework for interpreting our digital endocast. Our data illustrate new possibilities for shape and volumetric analyses, but are particularly impressive in demonstrating the potential of digital endocasts for interpreting circulatory, neural, and meningeal structures.

MATERIALS AND METHODS

The Scanned Specimen

San Diego Natural History Museum specimen SDSNH 21212 was collected at La Jolla Shores, San Diego County, CA, in October 1957, by R. M. Gilmore, where it presumably had stranded. The amount of time elapsed between death and collection is not recorded. The specimen was identified as *Tursiops gilli*, which is here considered to be synonymous with *Tursiops truncatus* (following Hansen, 1990, and Wells and Scott, 1999). This specimen is a representative of the "coastal form" of the bottlenose dolphin—a variety of the species that may eventually be accorded subspecific status (James Mead, personal communication). The specimen is male, with a skull length of 54.3 cm from the anterior-most rostrum to the occipital condyle. Other data regarding its age and life history are not available. The specimen has well-worn teeth, however, and many of its cranial sutures are completely closed, indicating its relatively advanced maturity. Apparently pathological bone growth is also visible externally on its posterior cranium.

Scanning

The specimen was scanned at the High-Resolution X-ray Computed Tomography Facility at The University of Texas at Austin (UTCT), which is described by Ketcham and Carlson (2001). The acquired slices were 1.0 mm thick, with an interslice spacing of 0.9 mm. The image field of reconstruction was 305.5 mm, and the reconstructed images were formatted as 1024 × 1024 16-bit TIFF files, resulting in an in-plane pixel resolution of 0.298 mm. A total of 628 images were obtained comprising the entire skull and mandibles, which were taped to the skull prior to scanning.

During the course of the scan there was an unexpected crash of the computer system. Several slices were corrupted, and were reacquired; all other images were "nudged" and rotated in Photoshop to account for their shifted position relative to those gathered before the crash. The reacquired images illustrated here include coronal slices 533–534 and 621–628. Note that it was impossible to reacquire these images at the precise level of the original series, introducing artifact into both sagittal and horizontal resliced images, as well as the 3D renderings of the skull and endocast. These artifacts only marginally affect the appearance of the digital endocast and the reslicings, and do not appreciably affect the endocranial volume estimates.

Visualization and Image Processing

We used VG Studio Max™ software for segmentation, visualization, and measurements. We individuated three main endocast segments (see Fig. 3), including a "neural" segment, a "circulatory" segment, and a "penetration" segment of the data comprising

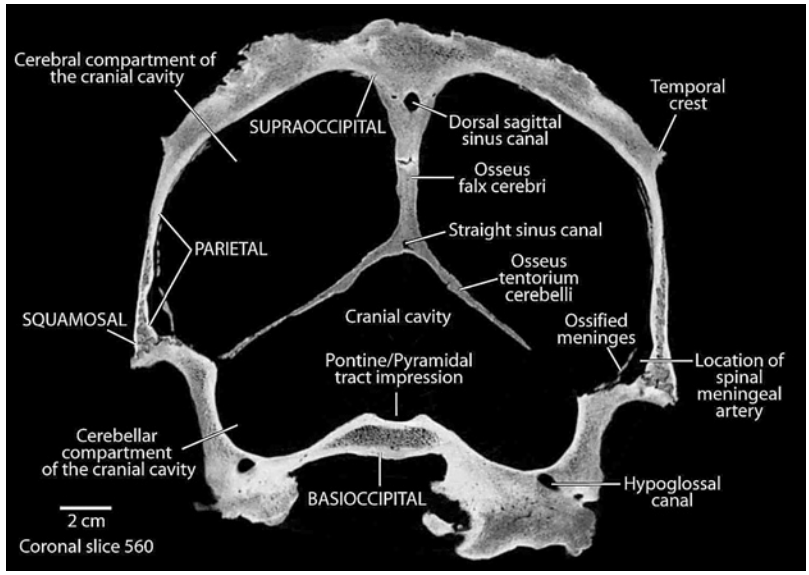

Fig. 2. Coronal slice 560, a representative CT slice from the original scan data.

casts of various canals and openings. These segments were manually selected using "magic wand" and "lasso" tools. Indicators for the limits of the neural spaces, circulatory spaces, and foramina within the cranial cavity and surrounding skeleton included sutures, marks, and indentations on the inner surface of the cranial cavity (e.g., Fig. 2). Both the falx cerebri and tentorium cerebelli are strongly ossified in this specimen, and they contain canals enclosing parts of the circulatory segment (Fig. 2). The circulatory segment was thus traced on the surface of our digitally rendered endocast as well as deeply within its volume, something that is not possible in natural endocasts. Meningeal membranes lining the roof and walls of the cranial cavity are also ossified, in both cerebral and cerebellar compartments (Fig. 2). These ossified membranes define epidural spaces within the cranial cavity that, in life, are primarily occupied by circulatory structures, such as hypertrophied retia mirabilia (e.g., McFarland *et al*., 1979). Similarly, canals and grooves in the bony walls of the cranium and ossified meninges are interpreted as representing traces of blood vessels. In places where the internal margins of vascular spaces were not defined by ossified meninges (such as the floor of the dorsal sagittal sinus sulcus), circulatory segments were selected to follow the contour of the brain surface as reflected on adjacent endocast surfaces.

The endocast was visualized with the skull rendered transparent, the "neural" segment colored pink, the "circulatory" segment red, and the "penetrations" segment blue (Figs. 1 and 3). We measured the volume of each segment. We also measured a reduced volume of the neural segment after contracting the segment by one pixel (one pixel equals approximately 0.4 mm), and again after contracting by two pixels, for reasons discussed below. Animations of the 3D endocast are available at the "additional imagery" page for *Tursiops truncatus* at www.digimorph.org.

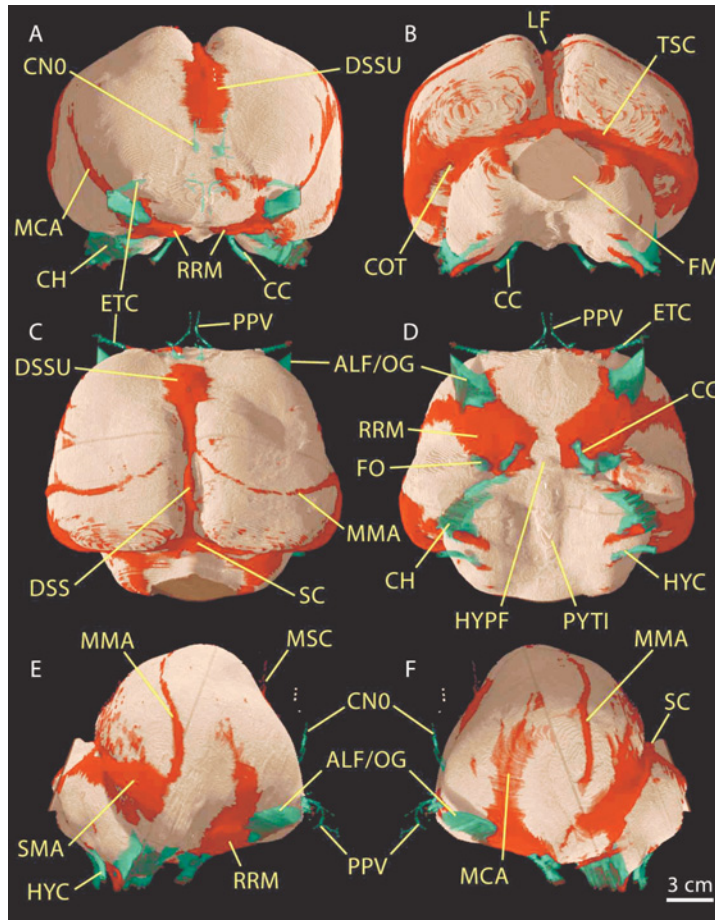

Fig. 3. 3D renderings of the cranial endocast, illustrating the various segmented components: (A) anterior view, (B) posterior view, (C) dorsal view, (D) ventral view, (E) right lateral view, and (F) left lateral view. Neural segment in pink, circulatory segment in red, and penetrations segment in blue. Abbreviations: ALF/OG: anterior lacerate foramen/optic groove; COT: cavity for osseous tentorium; CC: carotid canal; CH: cranial hiatus; MMA: middle meningeal artery; CN0: cranial nerve "0"; DSS: dorsal sagittal sinus; DSSU: dorsal sagittal sinus sulcus; FM: foramen magnum; FO: foramen ovale; HYC: hypoglossal canal; HYPF: hypophyseal fossa; LF: longitudinal fissure; MCA: middle cerebral arteries; ETC: ethmoidal canal; PPV: vessels that extend into the perpendicular plate of the ethmoid; PYTI: impression of the pyramidal tract; RRM: rostral rete mirabile; SC: sinus confluens; SMA: spinal meningeal arteries; TSC: transverse sinus canal.

Anatomical Nomenclature and Conventions

Terminology for nervous system anatomy generally follows Morgane and Jacobs (1972), terminology for circulatory system anatomy follows Geisler and Lou (1998), and skeletal terminology generally follows Rommel (1990). The following description often relates anatomical features to coded locations on the CT data (e.g., S143, H007, C343).

These codes refer to particular CT slices along the three main cranial axes in which structures appear. They are numbered sequentially from the front of the head (original coronal data, prefix "C," 0.9 mm interslice spacing), from the left side (digitally resliced sagittal set, prefix "S," 0.895 mm interslice spacing), and from the top (digitally resliced horizontal set, prefix "H," 0.895 mm interslice spacing). Numbered slices begin at a blank, air-only slice, which is immediately followed by a slice containing bone.

RESULTS

Description of the Cranial Endocast and the Cranial Cavity

The Endocast as a Whole

The neural segment comprises the majority of the endocast, and its overall shape resembles that of an isolated brain (Figs. 1 and 3). However, circulatory structures and meninges also occupy the endocranial cavity in life, and contribute to the surficial morphology of the endocast. Thus, for example, while the brain itself is highly gyrencephalic (Morgane *et al*., 1980), the smooth endocast surface reflects instead the inner surface of ossified and thickened meningeal membranes that covered the brain. Similarly, the ventral surface of the endocast bears casts of hypertrophied retia mirabilia (Melnikov, 1997; Geisler and Lou, 1998; see Circulatory Segment of the Endocast section later), and these largely obscure any surficial manifestation on the endocast of the olfactory lobes (not to be confused with the olfactory bulbs and tracts, which are absent in *Tursiops*; see Morgane *et al*., 1980) of the rhinencephalon and the optic chiasm. As discussed later, other blood vessels can be inferred elsewhere in our data volume.

Finally, canals and foramina for nerves and blood vessels are all represented as projections emanating from the endocast surface. The cetacean cranial hiatus is also rendered as a projection from the endocast surface. It represents a large gap between the bones surrounding the region of the embryonic metotic fissure, through which pass several cranial nerves and venous drainage of the brain surface.

"Neural" Segment of the Endocast

The overall neural endocast shape conforms well with published descriptions of the brain (e.g., Morgane and Jacobs, 1972; Morgane *et al*., 1980), being foreshortened and relatively wide. Reflecting the general odontocete condition, it lacks traces of olfactory bulbs and tracts (Fig. 3A). In life, a reduced rhinencephalon lies deep to the retia mirabilia, and thus would not be visible on the endocast.

By far the largest part of the neural segment is the diencephalic cortex. Unlike other mammals with large gyrencephalic brains, in which the endocranial surfaces preserve ridges that demarcate the sulci and gyri, the partially ossified meninges in *Tursiops* obscure impressions of these prominent features of the brain itself. Only a shallow, poorly defined trough on the lateral surface of the cerebral cast occupies a position over the Sylvian sulcus, which is a primary comparative neurological landmark (Morgane and Jacobs, 1972). The robust, ossified falx cerebri is represented by a deep longitudinal fissure in the mediposterior region of the cerebral cast. Rostrally, the anterior extent of the longitudinal fissure

corresponds to a major inflection of the endocast's dorsal contour (C493–548; Fig. 3E and F). The left hemisphere is slightly larger than the right at this level (see C520). The inflection is at the level of the frontal–supraoccipital suture, and the anterior extent of this suture is marked by the trace of the middle meningeal artery (described later; Fig. 3E and F). A distinct, spherical eminence representing the hypophyseal fossa occupies the center of the ventral surface of the endocast (C497–504; Fig. 3D), resting between casts of the carotid canals. The posterior margin of the hypophyseal fossa demarcates the cerebellar compartment of the endocast ventrally.

The cerebellar hemisphere casts are also quite prominent. They extend rostrally ventral to the temporal lobe casts, and posterolateral to the foramen ovale and carotid canal casts on either side. They are separated from the cerebral cast by a prominent transverse fissure, representing the cast of the osseus tentorium cerebelli (e.g., S190). The fissure is expressed on the surface of the endocast as deep pits on the margins of the transverse sinus canal cast described later (Fig. 3B).

On the ventral surface of the endocast the pons and pyramidal tract are represented by a broad, antero-posteriorly elongated elliptical cast between the casts of the two cerebellar hemispheres, immediately caudal to the hypophyseal fossa cast (C507–574, Fig. 3D). The cerebellum and brain stem casts extend caudally beyond the mass of the cerebral cast, and the cerebellar lobe casts extend slightly posterior to the level of the selected foramen magnum area in this endocast. The foramen magnum cast has a rounded diamond shape viewed posteriorly and is approximately 130% wider than it is high (Fig. 3B). The dorsal margin of the foramen magnum has a conspicuous notch expressed as a ridge on the endocast.

"Circulatory" Segment of the Endocast

Overall, the circulatory segment is bilaterally symmetrical. Traces of some vessels in the circulatory segment are located deep within the mass of the endocast, where they were conveyed by the ossified tentorium, and they are only visible when the neural segment of the digital endocast is rendered transparent.

The cast of the dorsal sagittal sinus is the most prominent circulatory feature seen on the dorsal surface of the cerebral portion of the endocast (Fig. 3C). The rostral portion of the dorsal sagittal sinus is not enclosed in a canal but rather a sulcus, which is expressed on the endocast as a swollen area immediately posterior to the terminal nerve canals (C470–490; Fig. 3C). Traces of small, paired canals marking the location of the closed ethmofrontal suture extend dorsally from the surface of this sulcus (see S148–151; Fig. 3E). Caudally, the sulcus diminishes, dipping into the longitudinal fissure (ca. C515–540) where it continues posteriorly as an irregular, arched, dorsal sagittal sinus canal cast (C542–583; S161–176). The dorsal sagittal sinus canal cast traverses the length of the longitudinal fissure. Small, often paired vessels occasionally exit the canal along its length (e.g., C572). Ultimately the dorsal sagittal sinus canal cast merges with the transverse sinus canal casts in a well-developed confluence of sinuses (C582–585; Fig. 3C).

The transverse sinus canal casts are prominent passages that lie above the transverse fissure (occupied by the ossified tentorium cerebelli). They occupy the surface of the endocast between the cerebrum and cerebellum, and are difficult to define lateral to the cranial hiatus (Fig. 3E and F).

The straight sinus canal cast is small, and extends rostrally through the ossified falx cerebri from the lower left confluence of sinuses (C580; see animations on digimorph.org). It gradually shifts from its location on the left side of the falx to a more central position (e.g., C561), and then angles dorsally onto the right side of the falx. Like the dorsal sagittal sinus canal cast, its anterior extent (C541–548) is located at the anterior end of the conjoined ossified tentorium and falx.

The middle meningeal artery casts follow the frontal–supraoccipital suture dorsally, where they occupy small grooves (Fig. 3C, E, and F). Dorsally, they reach or almost reach the anterior portion of the dorsal sagittal sinus cast. They arc posterolaterally, increase in volume as they course more directly ventrolaterally, and wrap laterally around the cerebral hemispheres above the temporal lobes. These meningeal vessels appear to issue from the internal extensions of the spinal meningeal arteries which are represented by textured surfaces overlying the temporal lobes. The posterodorsal corners of the internal extensions of the spinal meningeal arteries merge with the transverse sinus canal.

On the ventral surface of the endocast, the rostral rete mirabile (Geisler and Lou, 1998) is represented by an inflated region extending diagonally from the posteromedial margin of the anterior lacerate foramen toward the carotid canal, which emerges from the posteromedial extent of this raised surface (Fig. 3D). Note that the rostral rete mirabile has also been referred to as the internal carotid rete (Slijper, 1936; McFarland *et al*., 1979; Vogl and Fisher, 1981a,b); as the carotid rete (Melnikov, 1997); and as the internal ophthalmic rete (Galliano *et al*., 1966; Morgane and Jacobs, 1972; McFarland *et al*., 1979). Traces of thin vessels, presumably the middle cerebral arteries (McFarland *et al*., 1979), branch dorsally and posteriorly from the rostral rete cast, traversing the lateral surfaces of the endocast (Fig. 3F).

"Cranial Penetrations" Segment of the Endocast

The following describes casts of cranial penetrations seen from the most dorsal and rostral region of the endocast to the ventral and caudal end. The names of penetrations generally correspond to the nerves or structures that would have filled these spaces in life.

Casts of the small, dorsally trending canals of the terminal nerve, also known as Cranial Nerve 0, emerge just ventral to the anterior end of the dorsal sagittal sinus sulcus cast (C448–454, H78–107; Fig. 3A, E, and F; see Ridgway *et al*., 1987; Ridgway, 1990). They exit the skull toward the rear margin of the external nares (Rommel, 1990). Immediately anterior and ventral to the terminal nerve canal casts are traces of small, paired canals that extend into the mass of the perpendicular plate of the ethmoid (see C425–439, S150–179, H123–130). Lateral to these, extending laterally and slightly anteriorly, are the ethmoidal canal casts, which open onto the exterior of the skull as the ethmoidal foramina (Fig. 3A and C).

Casts of the confluent anterior lacerate foramina and optic grooves lie just below and lateral to the ethmoidal canal casts (Fig. 3D). These casts comprise robust, curved anteriorly extending penetrations. Casts of the optic grooves form their dorsolateral apex. Posteriorly, the anterior lacerate foramen casts are continuous with the rostral rete mirabile cast described earlier.

The carotid canal casts consist of long, narrow stalks that extend somewhat posterolaterally from the medioventral portion of the endocast surface (Fig. 3B). They are contained entirely within the basisphenoid (see C487–502). The foramen ovale casts are

seen immediately lateral and posterior to the carotid canal casts as thick, short stalks that extend laterally beneath the temporal lobes (see C494–510). The basisphenoid and basioccipital participate in the margins of these foramina. Their relative contributions are difficult to resolve, however, because these elements are completely fused in the scanned specimen.

The cranial hiatus (Rommel, 1990) casts record irregular openings posteromedial to the transverse fissure, and are bounded by the parietal, basioccipital, and exoccipital (Fig. 3D). The petrosal was not attached to the skull in this specimen, but would have occupied part of this space.

The casts of the hypoglossal canals emerge slightly posterior to the cranial hiatus casts, from the posteroventral surfaces of the cerebellar hemisphere casts (Fig. 3D and E). They extend slightly anteriorly and curve laterally. The basioccipital and exoccipital border the hypoglossal canals.

Volumetric Measurements

Volume estimates for the endocast segments and selected measurements are presented in Table II. These data indicate that the neural segment is by far the largest component of the endocast, representing 96% of the entire volume (neural + circulatory + penetrations segments). By contrast, the circulatory component comprises only 3% of the endocast volume.

DISCUSSION

Digital endocasts provide a unique source of data for interpreting endocranial anatomy. For example, they afford special information on the shape of the brain that may be lost in conventional anatomical preparations, and can provide accurate volumetric and linear measurements of certain gross regions of the brain and its related circulatory structures. The endocast only provides a reflection of the contents of the cranial cavity, however, and must be interpreted in this light.

The shape of the endocast reported here differs somewhat from published figures of isolated brains (e.g., Morgane and Jacobs, 1972; Morgane *et al*., 1980; Ridgway, 1990), as well as from MRI data of an isolated brain (Marino *et al*., 2001). Most notably, the endocast has a marked inflection of the dorsal contour viewed laterally, forming a low peak, anterior to which the dorsal cerebral cast has an almost planar surface that is interrupted medially by the dorsal sagittal sinus sulcus cast (see Fig. 2B). Published figures of brains and MRI data of isolated brains illustrate the dorsal contour to be a more evenly rounded surface (e.g., see Morgane and Jacobs, 1972, Fig. 29; Marino *et al*., 2001). Additionally, MRI data of an isolated brain (Marino *et al*., 2001), show the cerebral hemispheres touching along the length of the longitudinal fissure, and cerebrum and cerebellum touching in digitally resectioned imagery along the transverse fissure. The HRXCT endocast more accurately reflects the spatial separation between these lobes as defined by robust ossified falx cerebri and tentorium cerebelli, and may more accurately reflect the hydrostatic nature of the brain in life (Rowe, 1996a,b). These observed differences in shape most likely reflect distortion of isolated brains that have been removed from their supporting skeletal framework. Individual differences in maturity, sex, and overall body size may also affect the geometry of the brain within the skull. Note that the falx and tentorium ossify with age, and thus may not appear as a fissure in endocasts of young animals.

The HRXCT endocast does not record several features that are easily observed in conventional anatomical dissections and MRI data. For example, the rather smooth surface of the endocast does not reflect the inordinately gyrencephalic brain surface of *Tursiops*. Unlike published illustrations of dissected brains, the roots of the optic nerves are obscured, because hypertrophied retia mirabilia within the dura mater covers them. The cast of the hypophysis on the endocast is a small, spherical structure, whereas in illustrations of isolated brains it appears as a transversely elongated body (Morgane and Jacobs, 1972).

The circulatory segment of the virtual endocast of *Tursiops* compares quite favorably with published descriptions, and illustrates the potential of HRXCT to document such features in taxa for which conventional descriptions are not available. The major vessels on the surface of the brain could all be traced from grooves and canals on the endocranial walls. Contrary to Geisler and Lou (1998), there was evidence for the spinal meningeal arteries on the posterior cerebrum cast. As noted by Geisler and Lou (1998), however, many vessels do not have osteological correlates. Accordingly, the circulatory contribution to the endocast is underestimated because these could not be segmented (Table I). Attempting such segmentation using medical CAT scanning technology (e.g., Fig. 2) might compound this error, because their slices are thicker, and it is possible that many blood vessel traces would not be resolved. In any case, the estimates provided here indicate the relative magnitude of errors in estimating brain size using endocasts in which the circulatory component has not been isolated.

Comparison of the volumetric measurements of the neural segment indicates an extremely large brain (Table I). This volume is much larger than Marino *et al.*'s (2001) volume estimate based on MRI data for an isolated brain of an adult female specimen. They estimated the volume of the entire brain at 1363.13 cm^3, with a resulting estimate of whole brain weight of 1412.2 g (3% more than the fresh brain weight of 1378 g). However, the volume of the complete neural segment presented here may overestimate the actual brain volume of our specimen, because in addition to brain tissue, the neural segment also includes portions of the meninges that were not ossified, as well as the ventricular spaces within the brain. To account for the contribution of the non-ossified meningeal membranes to the whole volume, we additionally measured the volume of the neural segment after eroding its surface by 0.4 mm, and again after eroding its surface by 0.8 mm (the widths of one or two pixels, respectively). These erosions provide an approximation of the membrane thickness. The reduced volumes of the eroded endocast are still considerably larger than published estimates (e.g., Marino *et al.*, 2001; Glezer, 2002) and may indicate sexual or individual variation.

CONCLUSIONS

It has long been appreciated that mammalian endocasts are highly informative with respect to evolution of behavior, intelligence, sensory perception, locomotion, and other aspects of mammalian life history strategy (Jerison, 1973). This may be especially true in the case of cetaceans, whose evolutionary history saw marked enlargement of the brain (Marino *et al.*, 2004) and modulation in relative importance of its peripheral sensory systems, as well as profound modification of circulatory physiology. All of these features are reflected in the geometries and surfaces of the internal cavities and passageways of the skull, regions that have often been out of reach to scientists. Digital technologies for remote observation

of this part of the skull, together with informatics models to foster data dissemination and analysis (e.g., Rowe *et al*., 1999a,b), are bringing this fascinating realm into focus.

These data are particularly useful for revealing the shape of the brain, which is often distorted in conventional anatomical preparations when removed from its confining cranial cavity, and for their potential to trace components of the circulatory system that have osteological correlates. The results presented here demonstrate the potential of this technique to nondestructively reveal the generally inaccessible endocranial morphology of rare Recent and fossil taxa.

ACKNOWLEDGMENTS

Here's to Bill Clemens who, directly or indirectly, got us all interested in whale evolution and has stoked our enthusiasm in mammalian history for decades. Thanks to San Diego Natural History Museum and Tom Deméré and Kesler Randall for loaning the specimen that we scanned. Thanks also to Drs. Rich Ketcham and Julian Humphries, for advice in all aspects of scanning, data processing, and data interpretation, and to two anonymous reviewers and to David Polly for thoughtful reviews that improved this paper. This project was funded by NSF IIS IIS-9874781 and IIS-0208675 (to TR).

LITERATURE CITED

Barnes, L. G. (1985). Review: General features of the paleobiological evolution of Cetacea. *Mar. Mamm. Sci*. **1:** 90–93.

Breathnach, A. S. (1960). The cetacean central nervous system. *Biol. Rev. Camb. Philos. Soc*. **35:** 187–230.

Carlson, W. D., Rowe, T., Ketcham, R. A., and Colbert, M. W. (2003). Geological applications of high-resolution X-ray computed tomography in petrology, meteoritics and palaeontology. In: *Applications of X-Ray Computed Tomography in the Geosciences,* F. Mees, R. Swennen, M. Van Geet, and P. Jacobs, eds., vol. 215, pp. 7–22, Geological Society, London.

Conroy, G. C., and Vannier, M. W. (1984). Noninvasive three-dimensional computer imaging of matrix-filled fossils by high-resolution computed tomography. *Science* **226:** 456–458.

Edinger, T. (1955). Hearing and smell in cetacean history. *Monnatsschr. Psychiatr. Neurol*. **129:** 37–58.

Fordyce, R. E., and de Muizon, C. (2001). Evolutionary history of cetaceans: A review. In: *Secondary Adaptations of Tetrapods to Life in Water,* J.-M. Mazin and V. de Buffrenil, eds., pp. 16–233, Verlag Dr. Friedrich Pfeil, München, Germany.

Fraser, F. C., and Purves, P. E. (1960). Hearing in Cetaceans: Evolution of the accessory air sacs and the structure and function of the outer and middle ear in recent Cetaceans. *The Bulletin of the British Museum (Natural History) Zoology* **7:** 1–139.

Galliano, R. E., Morgane, P. J., McFarland, W. L., Nagel, E. L., and Catherman, R. L. (1966). The anatomy of the cervicothoracic arterial system in the bottlenose dolphin (*Tursiops truncatus*) with a surgical approach suitable for guided angiography. *Anat. Rec*. **155:** 325–338.

Geisler, J. H., and Lou, Z. (1998). Relationships of Cetacea to terrestrial ungulates and the evolution of cranial vasculature in Cete. In: *The Emergence of Whales,* J. G. M. Thewissen, ed., pp. 163–212, Plenum, New York.

Gingerich, P. D. (1998). Paleobiological perspectives on Mesonychia, Archaeoceti, and the origin of whales. In: *The Emergence of Whales*, J. G. M. Thewissen, ed., pp. 423–449, Plenum, New York.

Glezer, I. I. (2002). Neural morphology. In: *Marine Mammal Biology,* A. R. Hoelzel, ed., pp. 98–115, Blackwell, Oxford.

Glezer, I., Jacobs, M., and Morgane, P. (1988). Implications of the "initial brain" concept for brain evolution in Cetacea. *Behav. Brain Sci*. **11:** 75–116.

Hansen, L. J. (1990). California coastal bottlenose dolphins. In: *The Bottlenose Dolphin*, S. Leatherwood and R R. Reeves, eds., pp. 403–420, Academic Press, San Diego.

Jerison, H. J. (1973). *Evolution of the Brain and Intelligence*, Academic Press, New York.

Joeckel, R. M. (1998). Unique frontal sinuses in fossil and living Hyaenidae (Mammalia, Carnivora): Description and interpretation. *J. Vertebr. Paleontol*. **18:** 627–639.

Ketcham, R. A., and Carlson, W. D. (2001). Acquisition, optimization, and interpretation of X-ray computed tomographic imagery: Applications to the geosciences. *Comput. Geosci*. **27:** 381–400.

Leatherwood, S., and Reeves, R. R. (1990). *The Bottlenose Dolphin*, Academic Press, San Diego.

Marino, L., McShea, D. W., and Uhen, M. (2004). Origin and evolution of large brains in toothed whales. *Anat. Rec.* **281A:** 1247–1255.

Marino, L., Sudheimer, K. D., Murphy, T. L., Pabst, D. A., McLellan, W. A., Rilling, J. K., and Johnson, J. I. (2001). Anatomy and three-dimensional reconstructions of the brain of a bottlenose dolphin (*Tursiops truncatus*) from magnetic resonance images. *Anat. Rec.* **264:** 397–414.

Marino, L., Sudheimer, K. D., Sirpenski, G., and Johnson, J. I. (2003a). Neuroanatomy of the harbor porpoise (*Phocoena phocoena*) from magnetic resonance images. *J. Morphol.* **257:** 308–347.

Marino, L., Uhen, M. D., Frohlich, B., Aldag, J. M., Blane, C., Bohaska, D., and Whitmore, F. C., Jr. (2000). Endocranial volume of mid-late Eocene archaeocetes (Order: Cetacea) revealed by computed tomography: Implications for cetacean brain evolution. *J. Mamm. Evol.* **7:** 81–94.

Marino, L., Uhen, M. D., Pyenson, N. D., and Frohlich, B. (2003b). Reconstructing cetacean brain evolution using computed tomography. *Anat. Rec.* **272B:** 107–117.

McFarland, W. L., Jacobs, M. S., and Morgane, P. J. (1979). Blood supply to the brain of the dolphin, *Tursiops truncatus*, with comparative observations on special aspects of the cerebrovascular supply of other vertebrates. *Neurosci. Biobehav. Rev.* **3** (Suppl. 1): 1–93.

Melnikov, V. V. (1997). The arterial system of the sperm whale (*Physeter macrocephalus*). *J. Morphol.* **234:** 37–50.

Miller, G. S. (1923). The telescoping of the cetacean skull. *Smithsonian Misc. Coll.* **76:** 1–71.

Moore, W. J. (1981). *The Mammalian Skull*, Cambridge University Press, Cambridge.

Morgane, P. J., and Jacobs, M. S. (1972). Comparative anatomy of the cetacean nervous system. In: *Functional Anatomy of Marine Mammals*, Vol. 1, R. J. Harrison, ed., pp. 117–244, Academic Press, New York.

Morgane, P. J., Jacobs, M. S., and McFarland, W. L. (1980). The anatomy of the brain of the bottlenose dolphin (*Tursiops truncatus*). Surface configurations of the telencephalon of the bottlenose dolphin with comparative anatomical observations in four other cetacean species. *Brain Res. Bull.* **5:** 1–108.

Novacek, M. J. (1993). Patterns of diversity on the mammalian skull. In: *The Skull*, Vol. 2, J. Hanken and B. K. Hall, eds., pp. 438–545, University of Chicago Press, Chicago.

Ridgway, S. H. (1990). The central nervous system of the bottlenose dolphin. In: *The Bottlenose Dolphin*, S. Leatherwood and R. R. Reeves, eds., pp. 69–97, Academic Press, San Diego.

Ridgway, S. H., Demski, L. S., Bullock, T. H., and Schwanzel-Fukuda, M. (1987). The terminal nerve in odontocete cetaceans. *Ann. N. Y. Acad. Sci.* **519:** 201–212.

Rommel, S. (1990). Osteology of the bottlenose dolphin. In: *The Bottlenose Dolphin*, S. Leatherwood and R. R. Reeves, eds., pp. 29–49, Academic Press, San Diego.

Rowe, T. (1996a). Coevolution of the mammalian middle ear and neocortex. *Science* **273:** 651–654.

Rowe, T. (1996b). Brain heterochrony and evolution of the mammalian middle ear. In: *New Perspectives on the History of Life*, M. Ghiselin and G. Pinna, eds., pp. 71–96, California Academy of Sciences Memoir 20.

Rowe, T., Brochu, C. A., Kishi, K., Colbert, M., Merck, J. W., Jr., Saglamer, E., and Warren, S. (1999a). Alligator: Digital altas of the skull. Interactive multimedia on CD-ROM for Macintosh and PC computers. In: *Cranial Morphology of Alligator and Phylogeny of Alligatoroidae*, T. Rowe, C. A. Brochu, and K. Kishi, eds., Society of Vertebrate Paleontology Memoir 6.

Rowe, T., Brochu, C. A., Kishi, K., Colbert, M., and Merck, J. W., Jr. (1999b). Introduction to Alligator: Digital atlas of the skull. In: *Cranial Morphology of Alligator and Phylogeny of Alligatoroidae*, T. Rowe, C. A. Brochu, and K. Kishi, eds., pp. 1–8, Society of Vertebrate Paleontology Memoir 6. *J. Vertebr. Paleontol.* **19** (Suppl. 2).

Rowe, T., Carlson, W., and Bottorff, W. (1995). *Thrinaxodon: Digital Atlas of the Skull*. CD-ROM, 2nd edn. (for Windows and Macintosh platforms), University of Texas Press, 547 megabytes.

Rowe, T., Eiting, T., Macrini, T. E., and Ketcham, R. (2005). Osteology of the olfactory and respiratory systems in the nose of the opossum *Monodelphis domestica*. *J. Mamm. Evol.* **12:** 303–336.

Slijper, E. J. (1936). Die Cetaceen. Vergleichend-Anatomische und Systematisch. *Capita. Zoologica* **VI & VII:** 1–590.

Viamonte, M., Morgane, P. J., Galliano, R. E., and Nagel, E. L. (1968). Angiography in the living dolphin and observations on blood supply to the brain. *Am. J. Physiol.* **214:** 1225–1249.

Vogl, A. W., and Fisher, H. D. (1981a). The internal carotid artery does not directly supply the brain in the Monodontidae (Order Cetacea). *J. Morphol.* **170:** 207–214.

Vogl, A. W., and Fisher, H. D. (1981b). Arterial circulation of the spinal cord and brain in the Monodontidae (Order Cetacea). *J. Morphol.* **170:** 171–180.

Wells, R., and Scott, M. (1999). Bottlenose dolphin *Tursiops truncatus* (Montagu, 1821). In: *Handbook of Marine Mammals, Volume 6: The Second Book of Dolphins and the Porpoises*, S. Ridgway and Sir R. Harrison, eds., pp. 137–182, Academic Press, San Diego.